ELSEVIER

Journal of Magnetism and Magnetic Materials 221 (2000) 285–292

Journal of magnetism and magnetic materials

www.elsevier.com/locate/jmmm

Correlation between thermoelectric properties and magnetic phases in the charge-ordered $Pr_{0.5}Sr_{0.5-x}Ca_xMnO_3$

D. Niebieskikwiat, R.D. Sánchez[1,*]

Comisión Nacional de Energía Atómica-Centro Atómico Bariloche and Instituto Balseiro, 8400 Bariloche, Argentina

Received 31 May 2000

Abstract

We have performed measurements of thermoelectric power (TEP), electrical resistivity, DC magnetization and X-ray powder diffraction in polycrystalline samples of the charge-ordered manganite $Pr_{0.5}Sr_{0.5-x}Ca_xMnO_3$ for $x = 0, 0.1$ and 0.2. All the studied samples revealed three magnetic phases: paramagnetic at high temperatures, ferromagnetic below T_C down to T_N, below which the antiferromagnetic phase is established. At the paramagnetic–ferromagnetic transition, the TEP presents a clear break, and the three samples show metallic resistivity below T_C. On the other hand, below T_N all the samples turn to an insulating-like resistivity, but the TEP shows striking differences between the $x = 0$ sample and the other two. These differences are compatible with the different lattice and magnetic structures of the samples. These results support the idea that below T_N a 2D-metal is present and no charge-order accompanies the A-type antiferromagnetic phase.

PACS: 72.15.Jf; 71.30. + h

Keywords: Charge ordering; Thermoelectric power; Magnetic ordering

1. Introduction

Colossal magnetoresistance have been the most attractive property of the manganese oxides in the perovskite structure [1,2], but not the only one [3]. A rich relation between different structural, magnetic and electronic phases has created renewed interest because of the possibility of manipulating these properties. One of the most visited states of these materials is the charge-order (CO) state, where real-space periodic arrangement of Mn^{3+} and Mn^{4+} ions takes place [4]. This localization results in an abrupt increase in the resistivity and in most cases it is accompanied by the CE-type antiferromagnetic order [5].

As a fundamental parameter, the average ionic radius of the A-site in manganites ($\langle r_A \rangle$) drives the physical behavior of these compounds, i.e., for a given carrier concentration the strongest charge-ordered states are found for the lowest $\langle r_A \rangle$. As $\langle r_A \rangle$ decreases, the Mn–O–Mn bond angles decrease from the ideal 180° of the perovskite structure [6]. At the same time, the distortion of the MnO_6 octahedra for the Mn^{3+} ions increases and it stabilizes the Jahn–Teller (JT) distortions [7]. The increase in the local distortions induces carrier

* Corresponding author. Tel: + 54-2944-445274; fax: + 54-2944-445299.

[1] Member of CONICET, Argentina.

E-mail address: rodo@cab.cnea.gov.ar (R.D. Sánchez).

0304-8853/00/$ - see front matter
PII: S0304-8853(00)00500-X

localization, resulting in the CO state. The reduction in the mobility of the charge carriers also leads to the consequent reduction in the double-exchange mechanism [8], so at low temperatures the CO is accompanied by antiferromagnetic (AFM) order due to the super-exchange interaction [9].

Although the previous paragraph tends to describe the CO scenario in a simple way, the relation between the transport and magnetic properties are not totally clear. In fact, some compounds that present A-type antiferromagnetism at low temperatures are referred also as charge ordered [10,11]. However, in compounds like $Pr_{0.5}Sr_{0.5}MnO_3$, with A-type AFM order [12,13], scientists have not been able to establish the true electronic phase of the system at temperatures below T_N [10–14].

In this work we present measurements of the thermoelectric power (TEP), electrical resistivity, DC magnetization and X-ray powder diffraction in the $Pr_{0.5}Sr_{0.5-x}Ca_xMnO_3$ charge-ordered perovskite with $x = 0$, 0.1 and 0.2. We show that the electrical properties of this compound undergo an abrupt change when the Ca content increases. All the samples present a para-ferromagnetic transition at T_C and a ferro-antiferromagnetic transition at $T_N < T_C$. We have found that at T_N the sample with $x = 0$ presents qualitative differences in the TEP with respect to the other two samples. These differences are also seen in the lattice structure at room temperature, being tetragonal for $x = 0$ while for $x = 0.1$ and 0.2 we have found an orthorhombic structure. These results, together with that of the previous works of neutron diffraction [12,13], transmission electron microscopy (TEM) [13] and anisotropic resistivity [15] measurements, could be indicating the non-existence of a true charge-ordered state in A-type antiferromagnetic manganites. On the contrary, a 2D-metallic phase should be the associated electronic state.

2. Experimental

Powdered samples of $Pr_{0.5}Sr_{0.5-x}Ca_xMnO_3$ were prepared by the nitrate decomposition route. Raw materials were CO_3Sr, CaO and metallic Mn and Pr. The raw materials were mixed in the stoichiometric amounts and heated at 800°C in air for 12 h. Then the powders were pressed into pellets and treated at 1350°C for 12 h. A final heat treatment at 1450°C was performed for 12 h after an intermediate grinding. Finally, the samples were cooled down to 800°C at 5°C/min and then quenched to room temperature.

Powder X-ray diffraction (XRD) data were recorded on a Phillips PW 1700 diffractometer using $Cu\,K_\alpha$ radiation and a graphite monochromator. X-ray data at room temperature were refined by the Rietveld method with the fullprof program [16]. The magnetization (M) data were measured between 35 and 300 K in a commercial quantum design SQUID magnetometer with an applied magnetic field $H = 100$ Oe. The electrical resistivity ρ was measured by the usual four probe method in the 80–300 K temperature range with an applied current of 100 μA. The TEP coefficient (S) was measured in a home-made device with temperature gradients of ± 1.5 K between 80 and 300 K.

3. Results

3.1. X-ray diffraction

For the $x = 0$ sample, our refinement was made on the basis of the tetragonal $I4/mcm$ space group. On the other hand, the spectra of the $x = 0.1$ and 0.2 samples were refined in orthorhombic space groups. For $x = 0.1$, we have used the Ibmm space group, while for $x = 0.2$ the Pbnm space group provided the best fit of our data. The evolution of this system towards the Pbnm symmetry when x increases is an expected behavior, since for $x = 0.5$ the same space group was reported [17]. The obtained lattice parameters for the three samples are shown in Table 1.

In Fig. 1, we show the XRD pattern of the sample with $x = 0.2$ at room temperature. In the inset of this figure, the characteristic peak of the Pbnm space group present at $2\Theta = 25.9°$ is clearly observable, while it is not present in the X-ray patterns of the other samples.

Our XRD results are similar to that reported in previous works [13,17] and reflect an important difference between the samples. The tetragonal symmetry observed in the $x = 0$ sample is broken

Table 1
Room temperature lattice parameters, critical temperatures, average ionic radius and size mismatch of the A-site and band gap obtained from the high-temperature TEP of the $Pr_{0.5}Sr_{0.5-x}Ca_xMnO_3$ samples

Space group	$x = 0$	$x = 0.1$	$x = 0.2$
	$I4/mcm$	$Ibmm$	$Pbnm$
a(Å)	5.4135(6)	5.4688(7)	5.4507(4)
b(Å)	5.4135(6)	5.4335(7)	5.4240(4)
c(Å)	7.7895(9)	7.6340(9)	7.6450(6)
T_N(K)	138	189	178
T_C(K)	273	261	242
$\langle r_A \rangle$(Å)	1.244	1.231	1.218
$\sigma_A^2(10^{-3}Å^2)$	4.23	4.06	3.55
E_S(meV)	15.0	9.5	4.5

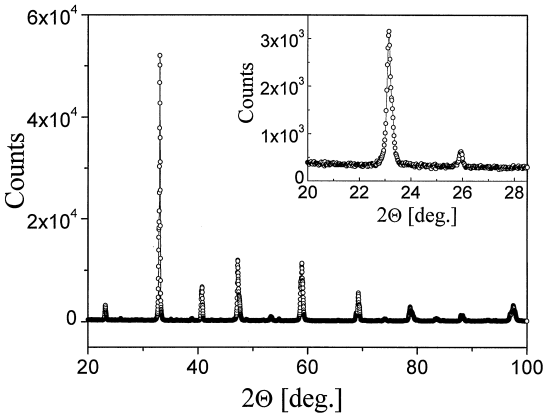

Fig. 1. Room temperature X-ray diffraction pattern of the $x = 0.2$ sample. The spectrum was adjusted assuming the orthorhombic Pbnm space group. Inset: blow up of the low angle region. The smaller peak at 25.9° is characteristic of the Pbnm symmetry.

into an orthorhombic one when the Sr atoms are replaced by smaller Ca atoms. This behavior is related to the stabilization of the local JT distortions when $\langle r_A \rangle$ is reduced. In the tetragonal $I4/mcm$ space group, the MnO_6 octahedra have only in-plane rotations (within the *ab* planes) while the angles along the *c*-axis are still 180° [13]. On the other hand, when smaller Ca atoms are added,

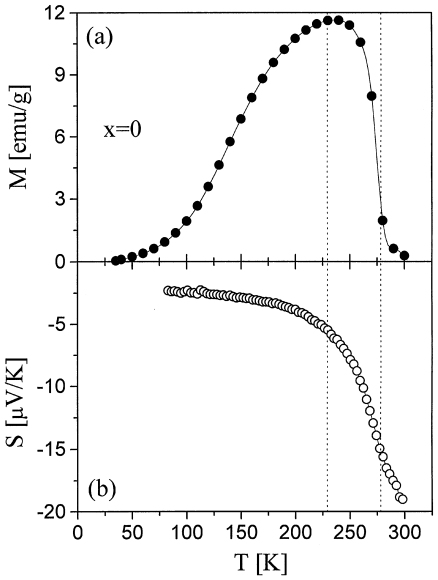

Fig. 2. (a) Magnetization vs. T for the Ca-free sample at $H = 100$ Oe. (b) TEP data as a function of temperature. A clear break is observed when ferromagnetic correlations begin to appear (as indicated by the dotted line). No features are observed at the FM – AFM transition.

tilts along the *c*-axis appear, changing the structure to the orthorhombic symmetry.

The homogeneity and the absence of secondary phases in the samples were checked in the XRD patterns and by SEM observations. SEM micrographs showed grains ranging from 2 to 4 μm in size.

3.2. Magnetization

The M vs. T curves were measured after the samples were cooled in zero magnetic field (ZFC), and can be seen in Figs. 2a, 3a and 4a for $x = 0$, $x = 0.1$ and $x = 0.2$, respectively. All the samples show two magnetic transitions on cooling: a paramagnetic (PM) to ferromagnetic (FM) one at T_C and a ferromagnetic to antiferromagnetic one at $T_N < T_C$. The critical temperatures, obtained as the position of the inflection points in the $M(T)$ curves, are displayed in Table 1. Although the $x = 0$ sample shows a broad transition at T_N, the Néel temperature is in agreement with the previous

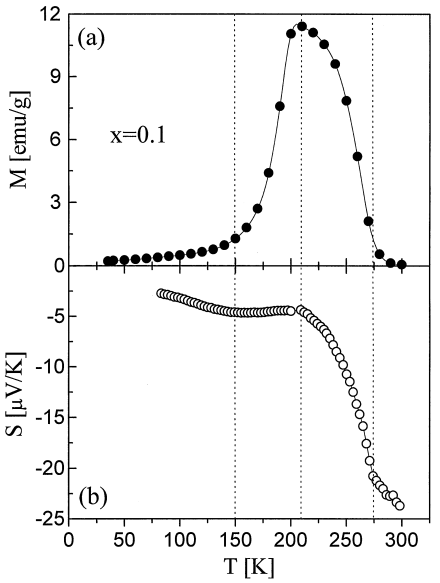

Fig. 3. (a) $M(T)$ curve at $H = 100$ Oe for the sample with $x = 0.1$. (b) S vs. T data. The wide *plateau* occurs around the transition from the FM to AFM charge-ordered state.

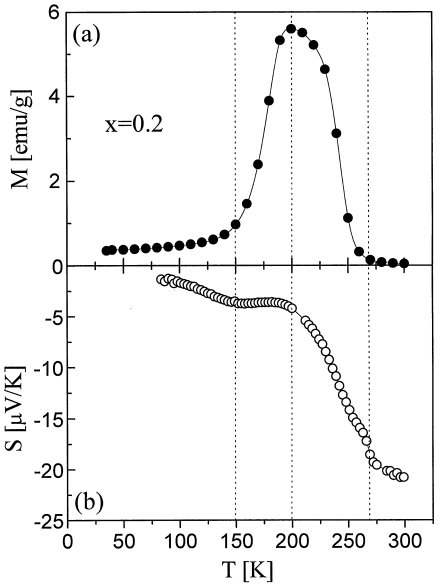

Fig. 4. (a) M vs. T data for the $x = 0.2$ sample with an applied magnetic field $H = 100$ Oe. (b) $S(T)$ curve. Note the change in the behavior of the TEP when the charge ordering is established below $T_N \approx 178$ K.

works [12]. The appearance of AFM interactions in $Pr_{0.5}Sr_{0.5}MnO_3$, that suppress the magnetization at high temperature well inside the FM phase (at $T \approx 230$ K) has also been observed [13].

It can be easily observed in Table 1 that the critical temperature T_C decreases while the Ca content x increases. This is an expected behavior due to the larger lattice distortion at higher x. The Mn–O–Mn bond angles decrease and the hopping probability is reduced, thus softening the double-exchange mechanism. On the contrary, the samples with $x = 0.1$ and 0.2 have a much higher T_N than the Ca-free sample.

3.3. Electrical properties

In Fig. 5 we show the ρ vs. T curves of the three samples. All of them present a metallic region at $T < T_C$, due to the FM order. On the other hand, below T_N the resistivity changes to an insulating behavior, with an appreciable hysteresis between the cooling and heating curves for $T < T_N$. Although similar features are presented by all the samples, we have to note in Fig. 5 that there exists some differences between the Ca-free sample and

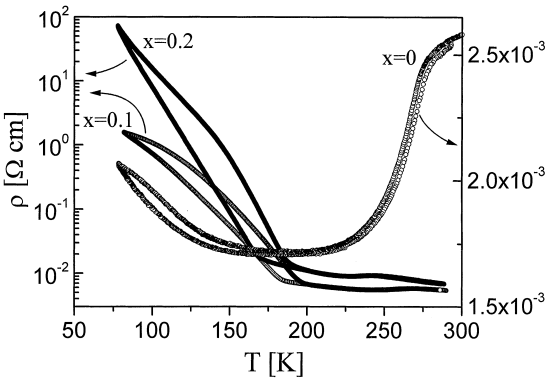

Fig. 5. Electrical resistivity of the three samples studied.

the other two. First, the change to an insulating-like resistivity in the sample with $x = 0$ is much more smooth than the step-like change in the samples with Ca. Second, the increase of ρ at $T < T_N$ in the $x = 0.1$ sample is of more than two orders of magnitude at 80 K, and the $x = 0.2$ sample has an increase of 10^4 at the same temperature. However, the $x = 0$ sample has a less marked increase of only 25%. Both these differences are as a consequence of

the different AFM structures presented by the samples. For $x = 0$ the compound exhibits an A-type AFM structure [12,13] and no charge ordering has been observed neither by neutron diffraction [12] nor by TEM studies [13]. On the other hand, for $x = 0.1$ the CE-type AFM structure realizes below T_N together with the appearance of charge ordering ($T_{CO} = T_N$) [18]. For $x = 0.5$ the AFM phase has also the CE-type structure and charge ordering appears at $T_{CO} > T_N$ in the PM phase [17]. Thus, for our $x = 0.2$ sample we expect the same AFM structure and also charge ordering, but with $T_{CO} = T_N$ because the temperature transition in the electrical resistivity coincides with T_N (see Fig. 4a).

In the lower panels of Figs. 2b, 3b and 4b , together with the magnetization curves we have plotted the S vs. T data. All the samples show a clear break at temperatures slightly above T_C, where ferromagnetic correlations begin to appear. This break implies a faster reduction of S (in absolute value) for $T < T_C$, that is related to the increase in the mobility of the charge carriers in the metallic phase. When T crosses T_N, the samples with $x = 0.1$ and 0.2 present a wide *plateau* while the AFM state is established. This behavior is related to the localization of the carriers due to charge ordering at T_N. On the other hand, the $x = 0$ sample shows no appreciable features at T_N, implying that the electronic state is not hardly affected by the magnetic transition, as it does occur with the other samples.

4. Discussion

The manganite $Pr_{0.5}Sr_{0.5}MnO_3$ (our $x = 0$ sample) has been previously studied on ceramic samples and single crystals. It is known that this compound exhibits two magnetic transitions. One from PM-insulator to FM-metallic at $T \approx 270$ K and a second one to AFM-insulator at $T \approx 140$ K. From the structural point of view, this perovskite is still a subject of controversy. Both Knížeck et al. [19] and Kawano et al. [12], at room temperature described the crystallographic phase with a Pbnm space group. By other way, Argyriou et al. [20] used a F4/mmc tetragonal symmetry and finally Damay et al. [13] made a systematic XRD, neutron diffraction and TEM study as a function of temperature and they explained the structure at 292 K with a tetragonal $I4$/mcm symmetry. The characteristic peak of the Pbnm orthorhombic space group, located at $2\Theta = 25.9^\circ$ in the spectrum of the $x = 0.2$ sample (see Fig. 1), did not appear in the spectrum of our Ca-free sample. Thus, in agreement with the results of Damay et al. [13], our best fit was obtained assuming the tetragonal $I4$/mcm space group.

From the electronic point of view, a more general controversy is still present in A-type AFM manganites. It is not clear whether or not the low-temperature AFM phase corresponds to a true charge-ordered phase in half-doped compounds. The $Pr_{0.5}Sr_{0.5}MnO_3$ manganite is included in this case, and the comparison of its electric properties with the other two samples, that indeed present charge ordering, gives striking differences at $T < T_N$.

Consistently with our resistivity and magnetization results, the TEP can be classified in several regions, as indicated by the vertical dotted lines in Figs. 2–4.

It is known that the TEP in manganites approaches a constant negative value at high temperatures [21]. Above T_C, a semiconducting behavior is observed because of the thermal activation of charge carriers, that determines the temperature dependence of the resistivity [22]. In this case, S can be described by

$$S = \frac{k_B}{e}\left(\frac{E_S}{k_B T} - B\right), \tag{1}$$

with E_S the band gap and the constant B (of the order of 1) is related to the spin [21] and configurational [23] entropies of the carriers, that determine the high-temperature TEP. In manganites $E_S \ll E_\sigma$, where E_σ is the band gap obtained from the electrical conductivity. This great difference between the values of the gap has been interpreted in the frame of strong electron–phonon coupling that forms small lattice polarons. Thus, the energy gap obtained from the conductivity is written as $E_\sigma = E_S + W_H$, where W_H is the energy barrier that the polarons must surpass in order to hop to

another site [22]. Therefore, the band gap of the TEP in this regime is insensitive to polaron parameters, as for example, the size or the effective mass (that generates the barrier W_H).

Despite of the small temperature range above T_C, we have estimated the values of E_S. These values are listed in Table 1, and are similar to that reported previously in other manganites [21,22,24]. As can be observed in Table 1, the value of E_S decreases with decreasing $\langle r_A \rangle$. Within the polaron frame, it is expected that the effective band gap behaves exactly in the opposite way. With decreasing $\langle r_A \rangle$ the structure stabilizes the JT distortions and therefore the polaron formation is favored, increasing its effective mass and producing localization of the charge carriers. This opposite behavior is an indication that the energy gap in the TEP does not sense polaron parameters above T_C. Thus, the observed behavior of E_S is perhaps related to the A-site size mismatch ($\sigma_A^2 = \langle r_A^2 \rangle - \langle r_A \rangle^2$), that introduces some disorder in the system. The ionic radius of the Sr^{2+} ions is much bigger than that of the Pr^{3+} ions. On the other hand, the Ca^{2+} and Pr^{3+} ions have the same ionic radius. In this way, when the Ca content x is increased $\langle r_A \rangle$ diminishes and σ_A^2 is also reduced, thus reducing the cationic disorder and, consequently, the electronic band energy gap E_S is also reduced [25,26].

At the temperatures where the ferromagnetic correlations begin to appear, a clear break in the $S(T)$ curves can be observed. These anomalies have also been observed in the previous TEP measurements in other ferromagnetic metallic manganites [24,27]. The faster decrease in the absolute value of S at lower temperatures is related to the rapid increase in the magnetization, with the consequent reduction in the magnetic scattering due to spin disorder. A maximum in $d|S|/dT$ is present at $T = T_C$, so that the variation of the TEP is given by the variation of M in the temperature region around T_C. This relation can be interpreted in terms of the magnetic scattering contribution to the conductivity. The general expression of the TEP is given by [28]

$$\sigma S = -\frac{1}{e}\int \frac{(\varepsilon-\mu)}{T}\sigma(\varepsilon)\left[-\frac{\partial f_0(\varepsilon)}{\partial \varepsilon}\right]d\varepsilon. \quad (2)$$

In this equation e is the electron charge, μ is the chemical potential, f_0 is the Fermi distribution, ε is the one-particle energy, σ is the conductivity and $\sigma(\varepsilon)$ is the energy-dependent conductivity, where the magnetic scattering plays a fundamental role. In the standard Boltzmann theory, making use of the relaxation time approximation

$$\frac{df}{dt} = \left(\frac{\partial f}{\partial t}\right)_{coll} = -\frac{f-f_0}{\tau(\varepsilon)}. \quad (3)$$

The term df/dt describes the evolution of the particles distribution function due to fields (electric field and temperature gradient) and the term $(\partial f/\partial T)_{coll}$ is related to the incoherent scattering, which returns the system to the equilibrium in a characteristic time $\tau(\varepsilon)$. By using standard procedures [28], from Eq. (3) we obtain

$$\sigma(\varepsilon) \propto e^2 v^2(\varepsilon)\tau(\varepsilon)N(\varepsilon), \quad (4)$$

where v is the velocity of the charge carriers and $N(\varepsilon)$ is the density of states. Thus, the key point determining the TEP is the energy and temperature dependence of the relaxation time $\tau(\varepsilon)$ and the density of states, around the Fermi level.

The TEP behavior in the ferromagnetic phase of all the studied samples do not show appreciable differences. This is not a surprising result, since the samples have the same magnetic structure (ferromagnetic), leading to a similar τ or scattering process. Also, the three samples show metallic $\rho(T)$ in this temperature range, so they must present half-filled conduction bands, with no gap at the Fermi level. Therefore, these similarities are reflected in the TEP.

Nevertheless, in the antiferromagnetic phase we expect different magnetic scattering for the samples with A- and CE-type magnetic structure. This different scattering mechanisms should affect the relaxation time $\tau(\varepsilon)$ and therefore also the TEP.

As can be seen in Fig. 2b, the TEP in the $x = 0$ sample is not greatly modified when the FM – AFM transition takes place. Thus, this transition to the AFM phase in the A-type structure does not strongly affect the mean free path of the charge carriers. This should be true at least in two dimensions, within the FM planes, where we expect the same high mobility of the carriers than in the 3D

FM phase. Also, a half-filled 2D conduction band is expected, similar to that of the 3D metallic state in the FM phase. This is indeed the result obtained in the mean-field theory. Maezono et al. [14] have shown that a 2D-metallic band, with $d_{x^2-y^2}$ orbital ordering, accompanies the A-type AFM order in half-doped manganites. This assumption would be false if a charge-ordered state were established below T_N, with the appearance of a band gap. However, in previous experiments of TEM [13] and neutron diffraction [12] on the $Pr_{0.5}Sr_{0.5}MnO_3$ manganite, no signals of charge ordering were observed. Moreover, anisotropic transport measurements in $Nd_{0.45}Sr_{0.55}MnO_3$ [15], that also presents A-type AFM order [12], show that the in-plane conductivity within the FM planes is 10^4 times higher than the out-of-plane conductivity at low temperatures. Thus, there are no reasons to assume the localized carriers within the FM planes in the A-type AFM structure. The weak semiconducting behavior presented by our $x = 0$ sample below T_N (Fig. 5) is related to its polycrystalline nature. In this resistivity measurement, a fraction of the out-of-plane conduction is included.

On the contrary, the other two samples with CE-type AFM structure present significant changes in the TEP around the FM–AFM transition at T_N. These changes indicate a different behavior of the carrier scattering, related to the appearance of a true charge-ordered phase below T_N. The transition zones observed in the TEP in Figs. 3b and 4b should occur when a band energy gap related to the charge ordered state develops in the density of states at the Fermi level. This gap turns the samples to a strong insulating phase, as shown by the resistivity curves in Fig. 5 for the $x = 0.1$ and 0.2 samples.

5. Conclusions

We studied $Pr_{0.5}Sr_{0.5-x}Ca_xMnO_3$ for $x = 0, 0.1$ and 0.2. At room temperature, important structural changes are observed when x increases. For the $x = 0$, 0.1 and 0.2 samples the space group are the tetragonal $I4/mcm$ and the orthorhombic Ibmm and Pbnm, respectively. Our thermoelectric power measurements show that all the samples behave in a similar way as in the paramagnetic and ferromagnetic phases. On the other hand, we found significant differences between the samples during the transition from a ferromagnetic to an antiferromagnetic state, when the temperature is decreased. The samples that exhibit CE-type magnetic structure and charge ordering ($x = 0.1$ and 0.2) present clear features at this magnetic transition, related to the change in the nature of the scattering processes and the appearance of a band gap in the density of states at the Fermi level. The $x = 0$ sample, that has A-type magnetic structure and no charge ordering, did not show appreciable changes at T_N. This behavior indicates that the scattering mechanism is hardly affected by the magnetic transition, and it should be related to the change from a 3D-metal in the ferromagnetic phase to a 2D-metal in the A-type antiferromagnetic phase.

Acknowledgements

This work was supported by CNEA (Argentine Atomic Energy Commission), CONICET (Argentine National Research Council), and Fundación Antorchas. We thank Dr. D.G. Lamas and L. Morales for their help with the XRD data. We acknowledge Dr. J. Sofo for the useful discussions about the TEP.

References

[1] R. Von Helmholt, J. Wecker, B. Holzapfel, L. Schultz, K. Samwer, Phys. Rev. Lett. 71 (1993) 2331.
[2] S. Jin, T. H. Tiefel, M. McCormack, R.A. Fastnacht, R. Ramesh, L.H. Chen, Science 264 (1994) 413.
[3] J.M.D. Coey, M. Viret, S. von Molnár, Adv. Phys. 48 (1999) 167.
[4] S. Mori, C.H. Chen, S.-W. Cheong, Nature London 392 (1998) 473.
[5] Y. Tokura, Y. Tomioka, J. Magn. Magn. Mater. 200 (1999) 1, and references therein.
[6] H.Y. Hwang, S.-W. Cheong, P.G. Radaelli, M. Marezio, B. Batlogg, Phys. Rev. Lett. 75 (1995) 914.
[7] H. Kuwahara, Y. Tomioka, A. Asamitsu, Y. Moritomo, Y.Tokura, Science 270 (1995) 961.
[8] C. Zener, Phys. Rev. 82 (1951) 403.
[9] J.B. Goodenough, Phys. Rev. 100 (1955) 564.
[10] Y. Tomioka, A. Asamitsu, Y. Moritomo, H. Kuwahara, Y. Tokura, Phys. Rev. Lett. 74 (1995) 5108.

[11] J. Wolfman, Ch. Simon, M. Hervieu, A. Maignan, B. Raveau, J. Solid State Chem. 123 (1996) 413.
[12] H. Kawano, R. Kajimoto, H. Yoshizawa, Y. Tomioka, H. Kuwahara, Y. Tokura, Phys. Rev. Lett. 78 (1997) 4253.
[13] F. Damay, C. Martin, M. Hervieu, A. Maignan, B. Raveau, G. André, F. Bourée, J. Magn. Magn. Mater. 184 (1998) 71.
[14] R. Maezono, S. Ishihara, N. Nagaosa, Phys. Rev. B 58 (1998) 11583.
[15] H. Kuwahara, T. Okuda, Y. Tomioka, A. Asamitsu, Y. Tokura, Phys. Rev. Lett. 82 (1999) 4316.
[16] Fullprof program, J. Rodriguez-Carvajal, Laboratoire Léon Brillouin (CEA–CNRS), v/October 1998.
[17] Z. Jirák, F. Damay, M. Hervieu, C. Martin, B. Raveau, G. André, F. Bourée, Phys. Rev. B 61 (2000) 1181.
[18] F. Damay, Z. Jirák, M. Hervieu, C. Martin, A. Maignan, B. Raveau, G. André, F. Bourée, J. Magn. Magn. Mater. 190 (1998) 221.
[19] K. Knížek, Z. Jirák, E. Pollert, F. Zounová, S. Vratislav, J. Solid State Chem. 100 (1992) 292.
[20] D.N. Argyriou, D.G. Hinks, J.F. Mitcell, C.D.Potter, A.J. Schultz, D.M. Young, J.D. Jorgensen, S.D. Bader, J. Solid State Chem. 124 (1996) 381.
[21] M.F. Hundley, J.J. Neumeier, Phys. Rev. B 55 (1997) 11511.
[22] M. Jaime, M.B. Salomon, K. Petit, M. Rubinstein, R.E. Treece, J.S. Horowitz, D.B. Chrisey, Appl. Phys. Lett. 68 (1996) 1576.
[23] P.M. Chaikin, G. Beni, Phys. Rev. B 13 (1976) 647.
[24] M.M. Savosta, J. Hejtmánek, Z. Jirák, M. Maryško, P. Novák, Y. Tomioka, Y. Tokura, Phys. Rev. B 61 (2000) 6896.
[25] R. Allub, B. Alascio, Phys. Rev. B 55 (1997) 14113.
[26] R. Allub, B. Alascio, Solid State Commun. 99 (1996) 613.
[27] J. Mira, A. Fondado, L.E. Hueso, J. Rivas, F. Rivadulla, M.A. López Quintela, Phys. Rev. B 61 (2000) 5857.
[28] R.D. Barnard, (Ed.), Thermoelectricity in Metals and Alloys, Taylor & Francis, London, 1972.